Int. J. Electrochem. Sci., 12 **(2017)** 4563 – 4573, doi: 10.20964/2017.05.84

International Journal of
ELECTROCHEMICAL
SCIENCE
www.electrochemsci.org

Facile Construction of MoS_2/CNFs Hybrid Structure for a Hydrogen Evolution Reaction

Jiang Li, WeiWei Wu, Meng Wan, Li Gu, Juan Wang, Tao Li, Han Zhu, Ming Zhang, MingLiang Du[*]

College of Materials and Textiles, Zhejiang Sci-Tech University, Hangzhou, 310018, P. R. China
[*]E-mail: du@zstu.edu.cn

Received: 16 June 2016 / *Accepted:* 11 January 2017 / *Published:* 12 April 2017

Development of high-efficiency electrocatalysts for a hydrogen evolution reaction (HER) is of great importance for the sustainable production of hydrogen that is necessary to relieve the energy crisis. Construction of a non-noble metal organic-inorganic hybrid structure with excellent HER activity is the key issue in electro-catalytic fields. Here, we demonstrate a facile synthetic route to prepare a flower-like MoS_2/CNFs hybrid structure with a high concentration of active edges sites using a hydrothermal method. The hybrid structure exhibits brilliant electro-catalytic performance in the HER process with an overpotential of 45 mV and the lower Tafel slope of 58 mV dec^{-1}, as well as a remarkable durability. The excellent HER activity of the MoS_2/CNFs hybrid structure is attributed to the high number of exposed active edges sites, high conductivity of carbon nanofibers (CNFs) and the high surface area of the CNFs mat.

Keywords: molybdenum disulfide; hydrothermal; carbon nanofibers; electrospinning; hydrogen evolution reaction

1. INTRODUCTION

Recently, the search for new energy alternatives to fossil fuels has been accelerated due to the energy dilemma and global warming [1, 2]. Sustainable and pollution-free hydrogen source has been recommended as a promising next-generation fuel that will succeed the current fossil fuels. Hydrogen production using the hydrogen evolution reaction that splits water into hydrogen and oxygen appears to be an efficient way for obtaining hydrogen, which is attracting intense research interest. To date, platinum, which meets almost all the requirements of the HER catalyst, still faces huge obstacles for its use in the HER because of its high cost and small reserves [3-6]. Therefore, development of Pt-free catalysts with high HER performance and low cost is still highly desired.

After decades of exploration, researchers found that the layered transition metal dichalcogenides (TMDs) (MX_2, where M =Mo, Co, W, and X=Se, S) have unique electronic properties and show remarkable electrochemical performance for the HER [7, 8]. Both theoretical calculations and experiments have verified that TMDs are highly efficient catalysts for the HER, with activities correlated with the amounts of active edges sites [9, 10]. Accordingly, constructing three-dimensional (3D) hierarchical TMDs with a high concentration of active edges sites has been identified as the feasible pathway for enhancing the HER performance [11, 12]. For instance, Li et al. designed MoS_2 nanoparticles anchored on reduced graphene using the solvothermal method and confirmed that hybrid structures can enhance the electro-catalytic performance in the HER activity[13]. Recently, Zou and Zhang successfully synthesized WS_2-carbon nanofiber mats with a novel 3D dendritic structures using the chemical vapor deposition (CVD) method, and found that these also exhibited a surprising electrochemical property [10].

Typically, catalytically active sites of MoS_2 located at the edges of the layered structures and, terminated with unsaturated sulfur atoms play a crucial role during the HER process [14, 15]. In addition to the active edges sites, high conductivity is another important and essential requirement for the HER. Because MoS_2 is a typical semiconductor, its low conductivity limits the electron transfer from electrodes to the active edges sites in the HER, thereby reducing the efficiency [16-18]. Construction of an electron highway by the introduction of conductive carbon based materials and a MoS_2 hybrid structure to decrease the electrode scattering is a superb approach for solving this problem [19, 20]. As is well known, carbon based materials with low cost, such as carbon nanotubes (CNTs) and carbon nanofibers (CNFs), are promising candidates for the construction of the hybrid structure due to their one dimensional morphology that allows electron transfer with low resistance along the axial direction. For instance, Wang's group reported that a few-layer MoS_2 coated on CNTs affords a low overpotential (90 mV) as well as a small Tafel slope (40 mv dec^{-1}) [21]. Xu's group prepared $WS_{2(1-x)}Se_{2x}$ with component-controllable nanotubes on CNFs that greatly exposed the active edges sites [22]. The excellent chemical and physical properties of CNFs have successfully attracted much attention due to their high conductivity and remarkable mechanical property, which are the two key factors for CNFs to be candidate of a substrate [23, 24]. What's more, the abundant precursor storage, facile preparation process and minimal environmental impact provide a potential possibility that CNFs can be widely used [25, 26]. Compared to CNTs, CNFs have some additional merits, including ultra-high axial length and controllable morphology. Currently, electrospinning is the most preferred technique for the preparation of successive CNFs with diameters down to the nanometer scale [27-29].

Herein, we designed a facile pathway to grow flower-like MoS_2 nanostructures anchored on CNFs with different ratios of molybdenum sources and CNFs. The CNFs were considered as a flexible substrate for the growth of flower-like MoS_2 nanostructures and lead to a faster charge transfer because of their high conductivity. The flower-like morphology not only provides sufficient surface areas, but also exposes more active edges sites for the HER. Hence, the interconnection between the high conductivity of CNFs and the exposed active edges sites of flower-like MoS_2, which are the two key factors affecting the electrochemical performance in the HER activity, were synergistically regulated.

The MoS_2/CNFs hybrid structure achieves a superior electro-catalyst performance for the HER including low onset overpotential (45 mV) as well as a small Tafel slope (58 mV dec^{-1}).

2. EXPERIMENTAL SECTION

2.1. Synthesis of polyacrylonitrile (PAN) nanofibers and CNFs

The PAN nanofibers were obtained using the electrospinning method. Typically, 1.93 g of PAN powders were dissolved in 15 ml of dimethyl formamide (DMF, 99.5%) and transferred into a flask under magnetic stirring to obtain homogenous solutions. Then, the solution was transferred into a medical syringe equipped using a stainless steel needle with an inner diameter of 15 mm. A static voltage (14 kV) was applied on the needle. The distance between the needle and the collecting plate that was covered with aluminum foil was adjusted to 12 cm, and the feeding rate was kept at 0.5 ml/h. The ambient temperature was maintained at 25±2 °C while the relative humidity was 45%.

The mats based on PAN nanofibers were cut into flakes and placed on a boat and then, placed into the CVD furnace for sintering. The mats were heated to 280 °C at the heating rate of 5 °C /min, and were maintained at 280 °C for 3 h in order to obtain sufficient pre-oxidation. Then, in the case of Ar with 150 sccm flow rate, the furnace was heated to 900 °C at the same heating rate and was maintained at that temperature for another 3 h in order to achieve the graphitization of the mats. Finally, the sample was cooled down to room temperature under the protection of Ar flow.

2.2. Hydrothermal preparation of MoS_2/CNFs

The hydrothermal route was adopted for the growth of MoS_2 on CNFs. Briefly, we controlled the ratio of ammonium molybdate and CNFs, and further regulated the morphology of products. Here, we chose three $(NH_4)_2MoO_4$: CNFs rations of 0.5:1, 1:1 and 2:1, denoted as bud MoS_2/CNFs (b-MoS_2/CNFs), flower-like MoS_2/CNFs (f-MoS_2/CNFs) and nanowalls MoS_2 (w-MoS_2/CNFs), respectively. For the synthesis of f-MoS_2/CNFs hybrids, 0.04 g of ammonium molybdate, 0.04 g of CNFs and 0.16 g of thiourea were dissolved in 35 ml of distilled water. After being shocked for several minutes, the solutions were transferred into a 50 ml capacity stainless steel autoclave with a Teflon inner tank and reacted at 210 °C for 24 h. Following the completion of the reaction, the autoclave naturally cooled to room temperature. The obtained products were washed several times alternately with water and ethanol, followed by drying in vacuum at 50 °C overnight. At this point, we have prepared f-MoS_2/CNFs hybrids. Correspondingly, b-MoS_2/CNFs and w-MoS_2/CNFs hybrids were prepared using the same synthesis routes.

2.3. Characterizations

The morphology and structure of the samples were characterized using transmission electron microscopy (TEM, JOEL JEM 2100F) at the acceleration voltage of 200 kV and scanning electron

microscopy (SEM) with a JSM-6700F FE-SEM (JEOL, Japan) at the acceleration voltage of 3 kV. The crystal structure is characterized using X-ray diffraction (XRD, Bruker AXS D8). The X-ray photoelectron spectra (XPS) measurements were recorded with an X-ray photoelectron spectrometer (Kratos Axis Ultra DLD) using a monochromatic Al K_α source (1486.6 eV). The electron dispersion spectroscopy (EDS) mapping images and high-angle annular dark field scanning TEM (HAADF STEM) images were obtained with an STEM (Tecnai G2 F30 S-Twin, Philips-FEI) at the acceleration voltage of 300 kV.

2.4. Electrochemical measurements

The electrocatalytic performance of the MoS_2/CNFs hybrids in the HER activity was tested using a three-electrode testing system using the CHI660b workstation in 0.5 M H_2SO_4 solutions. All obtained samples we cut into squares (1 cm × 1 cm) and clamped using a Teflon electrode. The catalysts act as the cathode material while Pt mesh acted as the counter electrode and the reference electrode is Ag/AgCl (E(RHE)) = E(RSC) + 0.244 V after standardizing). Cyclic voltammetry (CV) was performed to purge the surface and activate the catalyst following the Ar. Line sweep voltammetry (LSV) with the scan rate of 2 mV/s was conducted between +0.2 and -0.8 V vs RHE.

3. RESULTS AND DISCUSSION

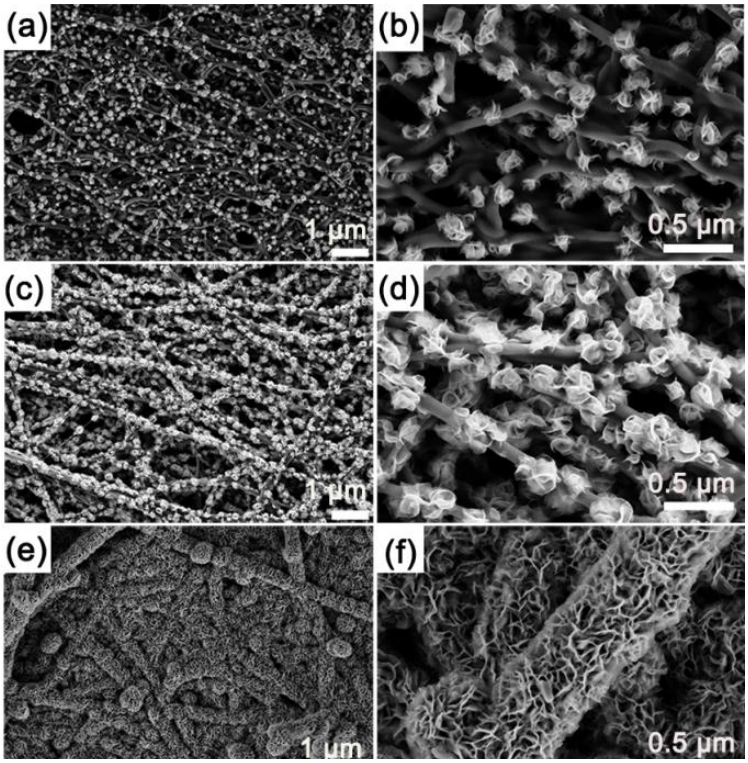

Figure 1. (a) and (b) FE-SEM image of b-MoS_2/CNFs. (c) and (d) FE-SEM image of f-MoS_2/CNFs. (e) and (f) FE-SEM image of w-MoS_2/CNFs.

The morphology of the as-prepared MoS_2/CNFs was investigated using FE-SEM. Here, Fig. 1 presents the images for the three different product ratios. Figs. 1a and 1b show the hybrid morphology of b- MoS_2/CNFs. It is apparent that the MoS_2 grew evenly on the CNFs and were prevented from agglomerating using CNFs in the process of reaction. It turns out that MoS_2 prefer to nucleate on CNFs with the crystal then growing along a certain direction, indicating the successful synthesis of the b-MoS_2/CNFs hybrids. The growth mechanism of the flower-like MoS_2 was suggested as follows [30]:

$$CH_3CSNH_2 + H_2O \rightarrow CH_3CONH_2 + H_2S \quad (1)$$

$$MoO_4^{2-} + 3H_2S \rightarrow MoS_2 + 3H_2 + SO_4^{2-} \quad (2)$$

Interestingly, with increasing molybdenum source content ($(NH_4)_2MoO_4$: CNFs =1:1), MoS_2 with flower morphology are dispersed uniformly onto the surface of nearly each CNFs, and a high number of MoS_2 layers with defect edges were exposed for better catalytic performance of the HER. As ratios were sequentially increased to 2:1, 3D flower-like MoS_2 change into grow on the surfaces of the MoS_2 nanowalls (Figs. 1e and 1f). It is evident that the CNFs are completely covered by the MoS_2 nanowalls. Moreover, when CNFs were completely wrapped by MoS_2 nanowalls, excess molybdenum sulfide formed spheroids morphology due to the insufficient carbon substrate. Furthermore, because the size of MoS_2 nanowalls became slightly larger, the carbon nanofibers were covered by MoS_2 nanowalls.

To further confirm the internal structure and the morphology of the as-prepared f-MoS_2/CNFs hybrids, the hybrid structure was also characterized using TEM. Fig. 2a shows the images of the MoS_2/CNFs hybrid, in which a single carbon nanofiber is covered with various blossoming flowers. The inset image (Fig. 2a) displays a vivid morphology about the flower-like MoS_2. The magnified TEM image presents the petals of f-MoS_2/CNFs, and more details are observed in Fig. 2b. As shown in Fig. 2c, it can be directly observed that only 4~6 layers of MoS_2 are present. The crystal lattice spacing of 0.273 and 0.645 nm is indexed to the [100] and [002] crystal orientations of MoS_2, respectively. The HRTEM image of the MoS_2 nanopetal shows a honeycomb-like arrangement of the atoms with a lattice spacing of 0.185 nm along the [105] crystal orientation of MoS_2 (Fig. 2d). The SAED pattern (insert in Fig. 2d) indicated that the obtained MoS_2 were polycrystalline.

The elemental distribution of f-MoS_2/CNFs is also investigated using HAADF-STEM and EDX. Fig. 3a shows STEM image of a MoS2/CNFs hybrid nanofiber. Fig. 3b reveals the high-resolution element mapping images that indicate the distribution of C, S and Mo elements. The distribution provides the evidence that the Mo and S elements are distributed homogeneously in the entire flower and further verifies the high purity of MoS_2. Fig. 3c depicts the EELS of the MoS_2, confirming the strong signals of Mo and S; the C element distribution is in good agreement with the diameter of CNFs, also implying that no C is doped into MoS_2 during the growth process. The EDX spectrum of MoS_2/CNFs shows the content of each element in the Fig. 3d. The atomic ratio of Mo and S is approximately 1:2.44, indicating that the synthesized MoS_2 is not stoichiometric. The unsaturated S atom ratio roughly demonstrates the existence of a large amount of MoS_2 active edges sites that is highly related to the HER performance.

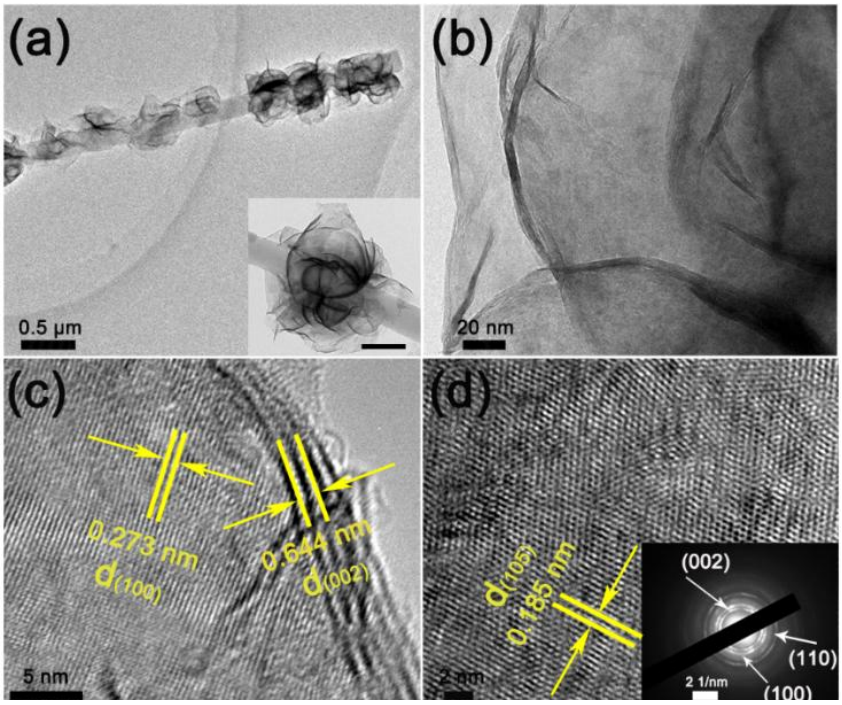

Figure 2. (a) TEM image of f-MoS_2/CNFs, inset: TEM image of f- MoS_2/CNFs. (b), (c) and (d) show HRTEM image of f-MoS_2/CNFs. The inset in (d) depicts the corresponding pattern obtained using selected area electron diffraction (SAED).

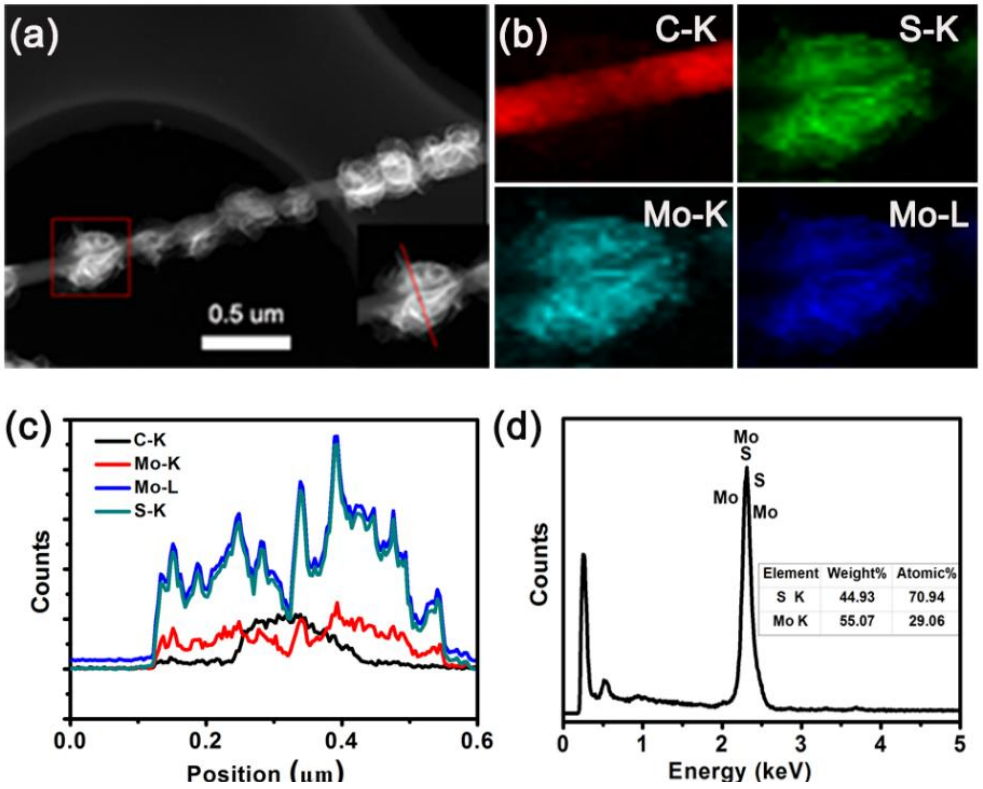

Figure 3. (a) HAADF STEM images of f-MoS_2/CNFs, inset: area of line-scan. (b) Corresponding distribution of the elements mapping in (a). (c) EELS spectra of the selected region in (a). (d) EDS spectra applied on the MoS_2/CNFs.

XPS was also carried out to analyze the chemical states of Mo and S on the surface of the MoS_2/CNFs hybrids. The XPS spectra of Mo 3d and S 2p are consistent with the characteristics of MoS_2. Fig. 4a shows two obvious peaks at 232.4 eV and 229.3 eV that are attributed to the Mo $3d_{3/2}$ and Mo $3d_{5/2}$, respectively, and are also ascribed to the Mo^{4+} of MoS_2 [31]. The binding energies of the S $2p_{1/2}$ and S $2p_{3/2}$ are 163.4 eV and 162.38 eV, corresponding to the S^{2-} of MoS_2 in Fig. 4b. Obviously, these investigations agree with the MoS2 crystal values reported in the literature [32, 33].

The XRD measurements were also performed to analyze the crystalline structure of the obtained materials with the measured pattern that is shown in Fig. 4c. All diffraction peaks can be indexed to the hexagonal 2H-molybdenite with lattice parameters a=3.14, b=3.14, c=12.53, and β=12.53°, corresponding to JCPDS card no. 75-1539. There are no impurity diffraction peaks indicating the high purity of the samples. All peaks show an obvious broadening caused by the small crystal size. Furthermore, the products with good crystallization may enhance their electrochemical stability in the acidic electrolytes. Otherwise, with the increasing concentration of ammonium molybdate and thiourea in growth solution, the intensity ratio of diffraction peak between MoS_2 and C gradually increases, in good agreement with the SEM images mentioned above. Additionally, Raman spectroscopy was applied to investigate the phase identity and compositions of the as-prepared f-MoS_2/CNFs as shown in Fig. 4d. The f-MoS_2/CNFs have two obvious characteristic signatures located at 380.4 cm^{-1} and 407.4 cm^{-1}, corresponding to the E_{2g} and A_{1g} modes, respectively. The in-plane E_{2g} mode can be attributed to the opposite direction of the vibration of Mo atom and the two S atoms while the vibrations of the A_{1g} mode are associated with the out-of-plane motion by S atoms only along the c-axis [34-36].

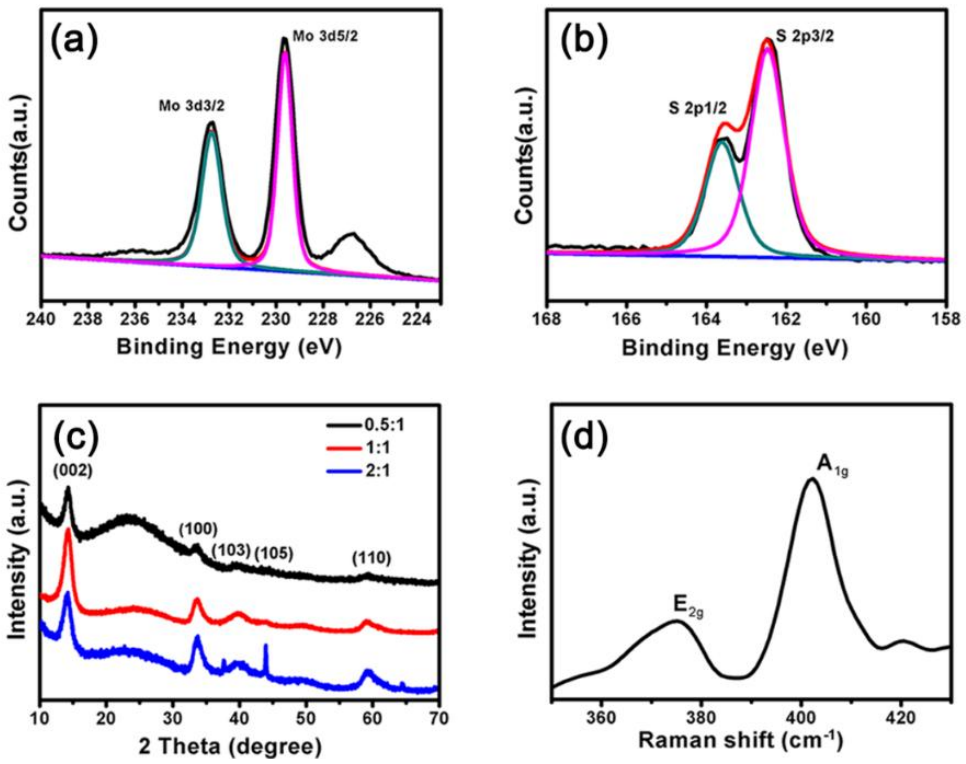

Figure 4. (a) and (b) XPS of Mo 3d and S 2p peaks taken from f-MoS_2/CNFs, respectively. (c) X-ray diffraction of various samples and (d) the Raman spectra of f-MoS_2/CNFs.

To confirm our expectations, the electrochemical performance of b-MoS_2/CNFs and f-MoS_2/CNFs as well as b-MoS_2/CNFs was investigated to assess the HER activity. As shown in Fig. 5a, pure CNFs manifest a high overpotential implying a poor HER activity, while Pt-C reveals an amazing HER activity. The f-/CNFs and w-MoS_2/CNFs show much lower onset potentials located at 45 mV and 40 mV, respectively. The current densities of f-MoS_2/CNFs and w-MoS_2/CNFs were clearly higher than that of b-MoS_2/CNFs. For example, the overpotential at 10 mA cm^{-2} is achieved at 75 mV for f-MoS_2/CNFs and w-MoS_2/CNFs, which is 3 times lower than that of b-MoS_2/CNFs (225 mV), indicating a higher HER activity. Ambrosi's group prepared hollow molybdenum sulfide to maximum expose active edge sites through template electrochemical fabrication. Typically, the decrease in size would improve the surface areas and lead to more active edge sites. However, as a semiconductor, the lower conductivity of MoS_2 limits the charge transfer to the cathode materials and reduces the HER activity, consequently, the overpotential at 10 mA cm^{-2} (202 mV) is approximately 3 times higher than that of f-MoS_2/CNFs (75 mV) [37]. The Guo and his co-works also reported molybdenum sulfide with similar nanostructure, with the onset overpotential at 112 mV, which is also much higher than that of the as-prepared f-MoS_2/CNFs [4]. In the present investigation, constructing an electron highway by CNFs can accelerate the electron transfer rate and is expected to significantly enhance the HER activity. The Tafel slope is associated with the inherent property of catalysts and, is calculated from Fig. 5a as presented in Fig. 5b. The calculated Tafel slope of the f-MoS_2/CNFs is 58 mV dec^{-1}, nearly equal to that of the w-MoS_2/CNFs (50 mV dec^{-1}), whereas the b-MoS_2/CNFs and pure CNFs show higher Tafel slopes of 161 mV dec^{-1} and 369 mV dec^{-1}, respectively. Yu *et al*. have spent lots of effort to investigate the layer-dependent of the electrochemical property of MoS_2 and Tafel slope is 142-144 mV dec^{-1} [38]. Li's group announced the MoS_2 nanoparticles grown on the graphene exhibiting much smaller Tafel slope (41 mV dec^{-1}) as lower as the f-MoS_2/CNFs (58 mV dec^{-1}) [39]. The small Tafel slope of f-MoS_2/CNFs implies a potential for practical applications, because such a small slope will lead to a higher HER rate with reduced overpotential [18]. As well known, the Tafel slope is significant property for the catalyst and it can be allowed to analyze the mechanisms of HER [40, 41]. The f-MoS_2/CNFs and w-MoS_2/CNFs share similar electrochemical performance in the HER activity, but the amount of ammonium molybdate precursor that is necessary for the synthesis of f-MoS_2/CNFs is only half of that needed for the synthesis of w-MoS_2/CNFs, indicating the higher HER of f-MoS_2/CNFs.

Durability and high HER activity are equally crucial for an outstanding catalyst. To probe the stability of f-MoS_2/CNFs, a long-term cycling measurement is carried out as presented in Fig. 5c. The excellent chemical durability of f- MoS_2/CNFs indicates that only negligible changes of HER performance relative to the initial performance in acidic environments occur even after 2000 CV cycles. To further evaluate the durability of the catalysts, an overpotential of 150 mV is applied constantly to maintain a current density 35 mA cm^{-2} for 12 h (Fig. 5d). We were gratified to observe that the f-MoS_2/CNFs hybrids still maintain an excellent electrochemical performance for HER because of the high exposed active edges sites as well as the compactly attached CNFs. In the present investigations, the excellent HER activity of the MoS_2/CNFs hybrid structure is mainly attributed to the many exposed active edges sites and high conductivity of CNFs. Additionally, the high surface

area of the CNFs mat is also responsible for the high electrocatalytic activity, by increasing the sufficient contact with the electrolyte.

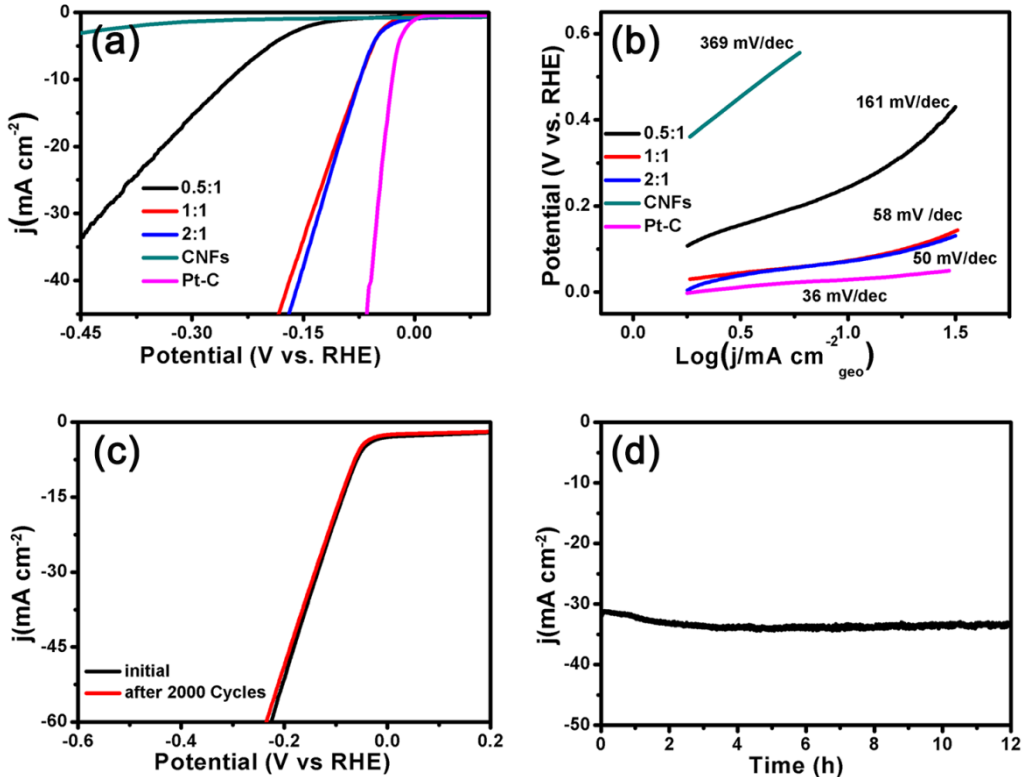

Figure 5. (a) Polarization curves of all samples after IR correction. (b) Tafel slope is calculated using (a). (c) and (d) the stability test of MoS_2/CNFs for the HER.

4. CONCLUSIONS

In summary, MoS_2/CNFs hybrid structures were successfully prepared using a facile hydrothermal route. The hierarchical structure with the high conductivity of CNFs that was constructed to expose more active edges sites was experimentally characterized and confirmed to result in significantly enhanced HER activity. The f-MoS_2/CNFs exhibit superior HER activity and high durability that is attributed to the high conductivity of the CNFs and the high concentration of the active edges sites. The present investigation describes a facile route to assemble MoS_2/CNFs hybrid structure with efficient HER property, that can also be applied in other fields such as lithium batteries and solar energy devices.

ACKNOWLEDGEMENTS
This study was supported by the National Natural Science Foundation of China (NSFC) (Grant number. 51373154, 51573166), the Program for Innovative Research Team of Zhejiang Sci-Tech University and the 521 Talent Project of Zhejiang Sci-Tech University.

References

1. S. Zhang, B. V. R. Chowdari, Z. Y. Wen, J. Jun and J. H. Yang, *ACS Nano*, 9(12) (2015) 12464-12472.
2. G. P. Bruce, B. Scrosati and J. M. Tarascon, *Angew Chem Int Ed*, 47(16) (2008) 2930-2946.
3. X. Dai, K. L. Du, Z. Z. Li, M. Z. Liu, Y. D. Ma, H. Sun, Y. Yang, *ACS Appl Mater Interfaces*, 7(49) (2015) 27242-27253.
4. B. J. Guo, K. Yu, H. L. Song, Y. Y. Zhang, X. Lei, H. Fu, Y. Y. Tan, Z. Q. Zhu, *ACS Appl Mater Interfaces*, 8(8) (2016) 5517-5525.
5. J. A. Turner, *Science*, 305(5686) (2004) 972-974.
6. M. Dresselhaus and I. Thomas, *Nature*, 414(6861) 332-337.
7. R. J. Bose, S. K.Balasingam, S. Shin, Z. Y. Jin, D. H. Kwon, Y. Jun and Y. S. Min, *Langmuir*, 31(18) (2015) 5220-5227.
8. S. Shin, Z. Jin, D. H. Kwon, R. Bose and Y. S. Min, *Langmuir*, 31(3) (2015) 1196-1202.
9. C. Tasi, K. Chan, F. Abild-Pedersen and J. K. Norskov, *Phys Chem Chem Phys*, 16(26) (2014) 13156-13164.
10. M. L. Zou, J. F. Zhang, H. Zhu, M. L. Du, Q. F. Wang, M. Zhang and X. W. Zhang, *J Mater Chem A*, 3(23) (2015) 12149-12153.
11. D. Y. Chung, S. K. Park, Y. h. Chung, S. H. Yu, D. H. Lim, N. Jung, H. C. Ham, H. Y. Park, Y. Z. Piao, S. J. Yoo and Y. E. Sung, *Nanoscale*, 6(4) (2014) 2131-2136.
12. X. L. Zheng, J. B Xu, K. Y. Yan, H. Wang, Z. L. Wang and S. H. Yang, *Chem Mater*, 26(7) (2014) 2344-2353.
13. Y. G. Li, H. L. Wang, L. M. Xie, Y. Y. Liang and H. J. Dai, *J Am Chem Soc*, 133(19) (2011) 7296-7299.
14. J. F. Xie, H. Zhang, S. Li, R. X. Wang, X. Sun, M. Zhou, J. F. Zhou, X. W. Lou and Y. Xie, *Adv Mater*, 25(40) (2013) 5807-5813.
15. J. J. Xie, J. J. Zhang, S. Li, F. Grote, X. D. Zhang, H. Zhang, R. X. Wang, Y. Lei, B. C. Pan and Y. Xie, *J Am Chem Soc*, 135(47) (2013) 17881-17888.
16. T. F. Jaramillo, K. P. Jorgensen, J. Bonde, J. H. Nielsen, S. Horch and I. Chorkendorff, *Science*, 317(5834) (2007) 100-102.
17. J. Kibsgaard, Z. B. Chen, B. N. Reinecke and T. F. Jaramillo, *Nat Mater*, 11(11) (2012) 963-969.
18. D. Merki and X. Hu, *Energy Environ Sci*, 4(10) (2011) 3878-3888.
19. J. Y. Kim, S. G. Byun, A. J. Smith, Jin. Y and J. X. Huang, *J Phys Chem Lett*, 4(8) (2013) 1227-1232.
20. M. L. Zou, Y. Jiang, M. Wang, M. Zhang, H. Zhu, T. T. Yang and M. L. Du, *Electrochim Acta*, 176 (2015) 255-264.
21. X. P. Dai, K. L. Du, Z. Z. Li, H. Sun, Y. Yang, W. Zhang ang X. Zhang, *Int J Hydrogen Energ*, 40(29) (2015) 8877-8888.
22. K. Xu, F. M. Wang, Z. X. Wang, X. Y. Zhan, Q. S. Wang, Z. Z. Cheng, M. Safdar and J. He, *ACS Nano*, 8(8) (2014) 8468-8476.
23. L. F. Zhang, A. Aboagye, A. Kelkar, C. L. Lai and H. Fong, *J Mater Sci*, 49(2) (2014) 463-480.
24. F.Gardea, M. Naraghi and D. Lagoudas, *Appl Mater Interfaces*, 6(2) (2014) 1061-1072.
25. Z. Y. Wu, C. Li, H. W. Liang, J. F. Chen and S. H. Yu, *Angew. Chem.* 125(10) (2015) 2997-3001
26. X. Z. Xu, J. Zhou, L. Jiang, G. Lubineau, S. A. Payne and D. Gutschmidt, *Carbon*, 80 (2014) 91-102.
27. H. Hou and D. H. Reneker, *Adv Mater*, 16(1) (2004) 69-73.
28. A. Greiner and J. H. Wendorff, *Angew Chem Int Ed*, 46(30) (2007) 5670-5703.
29. L. Matlock-Colangelo, D. W. Cho, C. L. Pitner, M. W. Fery and A. J. Baeumner, *Lab chip*, 12(9) (2012) 1696-1701.
30. J. Wang, J. L. Liu, J. S. Luo, P. Liang, D. L. Chao, L. F. Lai, J. Y. Lin and Z. X. Shen, *J. Mater.*

Chem. A, 3(34) (2015) 17534-17543..
31. Q. H. Liu, Z. J. Wu Z. L. Ma, S. Dou, J. H. Wu, L. Tao, X. Wang, C. B. Ouyang. A. L. Shen and S. G. Wang, *Electrochim Acta*, 177 (2015) 298-303.
32. V. O. Koroteev, L.G. Bulusheva, I. P. Asanov, E. V. Shlyakhova, D. V. Vyalikh and A. V. Ootrub, *J Phys Chem C*, 115(43) (2011) 21199-21204.
33. S. B. Yang, L. J. Zhi, K. Tang, X. L. Feng, J. Maier and K. Müllen, *Adv Funct Mater*, 22(17) (2012) 3634-3640.
34. C. G. Lee, H. G. Yan, L. E. Brus, T. F. Heinz, J. Hone and S. M. Ryu, *ACS Nano*, 4(5) (2010) 2695-2700.
35. B. J. Cho, J. W. Yoon, S. K. Lim, A. R. Kim, D. H. Kim, S. G. Park, J. D. Kwon, Y. J. Lee, K. H. Lee, B. H. Lee, H. C. Ko and M. G. H, *ACS Appl Mater Interfaces*, 7(30) (2015) 16775-16780.
36. C. Ataca, M. Topsakal, E. Aktürk and S. Ciraci, *J Phys Chem C*, 115(33) (2011) 16354-16361.
37. A. Ambrosi and M. Pumera, *ACS Catal.* 6(6) (2016) 3985-3993.
38. Y. F. Yu, S. Y. Huang, Y. P. Li, S.N. Steinmann and L. Y. Cao, *Nano Lett.* 14(2) (2014) 553-558.
39. Y. G. Li, H. L. Wang, L. M. Xie, Y. Y. Liang, G. S. Hong and H. J. Dai, *J Am Chem Soc*, 133 (2011) 7296-7299.
40. J. O. M. Bockris and E. C. Potter, *J. Electrochem. Soc*., 99 (1952) 169–186.
41. J. G. Thomas, *Trans. Faraday Soc.*, 57 (1961) 1603-1611.